Validation of an accelerated "Demons" algorithm for deformable image registration in radiation therapy

Article *in* Physics in Medicine and Biology · July 2005

Impact Factor: 2.76 · DOI: 10.1088/0031-9155/50/12/011 · Source: PubMed

10 authors, including:

Lei Dong
Scripps Health
386 PUBLICATIONS **7,796** CITATIONS
SEE PROFILE

Radhe Mohan
University of Texas MD Anderson Cancer Ce…
303 PUBLICATIONS **12,809** CITATIONS
SEE PROFILE

Deborah A Kuban
University of Texas MD Anderson Cancer Ce…
346 PUBLICATIONS **11,836** CITATIONS
SEE PROFILE

Joe Y Chang
University of Texas MD Anderson Cancer Ce…
280 PUBLICATIONS **4,771** CITATIONS
SEE PROFILE

INSTITUTE OF PHYSICS PUBLISHING PHYSICS IN MEDICINE AND BIOLOGY

Phys. Med. Biol. **50** (2005) 2887–2905 doi:10.1088/0031-9155/50/12/011

Validation of an accelerated 'demons' algorithm for deformable image registration in radiation therapy

He Wang[1], Lei Dong[1], Jennifer O'Daniel[1], Radhe Mohan[1], Adam S Garden[2], K Kian Ang[2], Deborah A Kuban[2], Mark Bonnen[2], Joe Y Chang[2] and Rex Cheung[2]

[1] Department of Radiation Physics, The University of Texas MD Anderson Cancer Center, 1515 Holcombe Blvd, Houston, TX 77030, USA
[2] Department of Radiation Oncology, The University of Texas MD Anderson Cancer Center, Houston, TX, USA

E-mail: ldong@mdanderson.org

Received 31 January 2005, in final form 19 April 2005
Published 1 June 2005
Online at stacks.iop.org/PMB/50/2887

Abstract

A greyscale-based fully automatic deformable image registration algorithm, originally known as the 'demons' algorithm, was implemented for CT image-guided radiotherapy. We accelerated the algorithm by introducing an 'active force' along with an adaptive force strength adjustment during the iterative process. These improvements led to a 40% speed improvement over the original algorithm and a high tolerance of large organ deformations. We used three methods to evaluate the accuracy of the algorithm. First, we created a set of mathematical transformations for a series of patient's CT images. This provides a 'ground truth' solution for quantitatively validating the deformable image registration algorithm. Second, we used a physically deformable pelvic phantom, which can measure deformed objects under different conditions. The results of these two tests allowed us to quantify the accuracy of the deformable registration. Validation results showed that more than 96% of the voxels were within 2 mm of their intended shifts for a prostate and a head-and-neck patient case. The mean errors and standard deviations were 0.5 mm $\pm$ 1.5 mm and 0.2 mm $\pm$ 0.6 mm, respectively. Using the deformable pelvis phantom, the result showed a tracking accuracy of better than 1.5 mm for 23 seeds implanted in a phantom prostate that was deformed by inflation of a rectal balloon. Third, physician-drawn contours outlining the tumour volumes and certain anatomical structures in the original CT images were deformed along with the CT images acquired during subsequent treatments or during a different respiratory phase for a lung cancer case. Visual inspection of the positions and shapes of these deformed contours agreed well with human judgment. Together, these results suggest that the accelerated demons algorithm has significant potential for

delineating and tracking doses in targets and critical structures during CT-guided radiotherapy.

(Some figures in this article are in colour only in the electronic version)

1. Introduction

Recent advances in three-dimensional conformal radiotherapy (3DCRT) and intensity-modulated radiation therapy (IMRT) allow more precise tumour targeting and preservation of normal tissues (Ezzell *et al* 2003, Mackie *et al* 2003). However, this precision may be adversely affected by changes in the location, shape and size of tumours and normal anatomy during the normal course of radiation treatments. To ensure that the prescribed dose is delivered to the clinical target volume (CTV), additional margins are commonly added to the CTVs to form a planning target volume (PTV). The PTV margin accounts for uncertainties due to set-up, organ motion and target deformation (Stroom and Heijmen 2002). However, this additional margin significantly increases the treated volume and may increase radiation toxicity to surrounding critical non-target organs. On the other hand, many investigators have also expressed concern that, when reduced margins are used, there may be geometric miss of the target volumes during daily radiation delivery.

Soft tissue deformations can be caused by daily physiological changes (e.g. bladder filling or changes in rectal contents) or clinical factors (e.g. weight loss or tumour shrinkage). The anatomy delineated during treatment planning prior to treatment may not adequately account for inter-fractional changes and may even limit the potential of highly conformal treatment modalities such as IMRT (Li and Xing 2000, Samuelsson *et al* 2003, Hector *et al* 2000). Furthermore, the shape and location of intra-thoracic tumours could vary in different phases of a respiratory cycle. A deformable image registration algorithm may also help to track these changes if four-dimensional time-sequenced CT images are available.

Daily CT imaging can now be readily accomplished in the same room as the linear accelerator (Mackie *et al* 2003, Jaffray *et al* 2002, Fung *et al* 2003, Court *et al* 2003). For example, the CT-on-Rails system uses the same couch for both imaging and treatment (Court *et al* 2003, 2004 Court and Dong 2003). On-board cone-beam CT or integrated tomotherapy units are available for in-room CT-guided radiotherapy (Sidhu *et al* 2003, Ford *et al* 2002, Jaffray and Siewerdsen 2000, Jaffray *et al* 2002, Mackie *et al* 2003).

To quantify and track time- and position-dependent variations in patient anatomy, deformable image registration is necessary to map the position of each volume element (voxel) to a reference CT image for dose tracking or replanning (Yan *et al* 1999, Lockman *et al* 2000, Liang and Yan 2003, Brock *et al* 2002, 2003, Meyer *et al* 1997, Joshi *et al* 2002, Joshi and Miller 2000, Valverde *et al* 2001, Metaxas and Kakadiaris 2002, Tichavsky and Wong 2002, Thirion 1996, 1998). However, deformable registration algorithms have not been extensively evaluated or validated. Therefore, in the present study, we evaluated an 'active force' demons algorithm for its ability to track deformations in both mathematically deformed patient images and physically deformed phantom studies. We also explored the application of using the demons algorithm for auto-segmentation of patient's anatomy in subsequent CT images of the same patient.

2. Methods and materials

2.1. 'Demons' algorithm

Deformable (non-rigid) image registration algorithms can be categorized into two classes: feature-based or greyscale image-based. Feature-based algorithms match contours, fiducial points or landmark points and lines in the deformed image with the same features in the reference image either manually or automatically. Potential errors in feature detection may be carried over into the deformable image registration process. In addition, extra time for extracting features before image registration may be needed (for example, manual delineation of feature points can be time consuming). In contrast, greyscale image-based algorithms use pixel or voxel data directly, assuming that image intensities alone contain enough information for image registration. Usually, the feature-based algorithms are faster than image intensity-based algorithms when performing image registration because they usually operate on a sparse set of features. However, the time spent on feature extraction can be significant and error prone.

CT images are used in calculating radiation doses because Hounsfeld units (CT pixel values) are calibrated to the attenuation coefficient of water and therefore the pixel values are well defined. Because of the consistency in CT image intensities, it is advantageous to use a greyscale image-based algorithm for radiotherapy applications. The method we implemented was primarily based on Thirion's diffusing model, also known as the 'demons' algorithm (Thirion 1998, Tichavsky and Wong 2002).

The original 'demons' algorithm used gradient information from a static reference image to determine the 'demons' force required to deform the 'moving' image. This may not be efficient, especially when the gradient on the reference image is low. Conceptually, the diffusing model assumes that local 'demons' at every voxel location are applying invisible 'forces' that push the voxels of the moving image into matching up with the reference (static) image. The original 'demons' algorithm was studied by several authors using simulated images or medical images (especially brain images) (Xie *et al* 2003, Guimond *et al* 2001, Cachier *et al* 1999). In these studies, the optical flow formula was used to estimate the 'demons' forces either at image feature points or at voxel positions on a greyscale image.

2.2. Demons force calculation

The optical flow equation was used to estimate demons forces. For a given point P, let s be the intensity in static image S and m the intensity of the moving image M. The estimated displacement $\vec{u}$ required for point P to match the corresponding point in M is given by (Thirion 1998)

$$\vec{u} = \frac{(m-s)\vec{\nabla}s}{|\vec{\nabla}s|^2 + (m-s)^2} \tag{1}$$

where $\vec{u} = (u_x, u_y, u_z)$, and $\vec{\nabla}s$ is the gradient of the static image. $\vec{\nabla}s$ represents the relationship between the neighbouring points in the static image (analogue to automatically generated features by edge enhancement); thus, it is an 'internal' force originating from the static image. The $(m-s)$ term is the differential force of the interaction between the static and the moving images; hence, it is an 'external' force.

Equation (1) is calculated iteratively in the original 'demons' algorithm (Thirion 1998). In each iteration, the optical flow computation is followed by regularization of the deformation field using a Gaussian filter with a variance of σ^2. Since the displacement is calculated from local image information only, the regularization is essentially a smoothing operation to

suppress noise and preserve the geometric continuity of the deformed image. Bro-Nielsen and Gramkow (1996) demonstrated that the Gaussian filtering used in the 'demons' algorithm approximates the linear elastic filter used in the viscous fluid model for deformable image registration. In addition, the body force, estimated by equation (1), is almost identical to their fluid model.

2.3. Addition of active force to diffusion process

It can be seen from equation (1) that the gradient information that drives the deformation is inefficiently taken from the static image only. Registration may be made more efficient, however. Assuming that diffusion is bi-directional, 'demons' at any point in the image space will produce not only a force that allows a deformable 'moving' object to diffuse into a corresponding 'static' object, but also produce a force that allows the 'static' object to diffuse into the corresponding 'moving' object. Rogelj and Lovacic (2003) demonstrated a similar idea when they investigated the quality of image matching with a similarity-based non-rigid registration algorithm. They added to the deformable image a new force based on Newton's third law of motion, which states that forces on one image reflect opposing forces on the other image. They also proved experimentally that when both images were treated in the same manner, the consistency and registration correctness improved. Similarly, we added a new force to the 'demons' algorithm. However, since we wanted to deform one of the images (the moving image), the new force was applied to the deformed image (moving image) only.

Another equation, similar to equation (1), was used to define an 'active' force $\vec{f}_m$ based on the gradient information of the moving image:

$$\vec{f}_m = -\frac{(s-m)\vec{\nabla}m}{|\vec{\nabla}m|^2 + (s-m)^2} \tag{2}$$

where '-' indicates an opposing force. Combining the 'passive' force $\vec{f}_s$ (defined as the right side of equation (1)) and the 'active' force $\vec{f}_m$ in equation (2), the total force at point P can be calculated as

$$\vec{f} = \vec{f}_s + \vec{f}_m = (m-s) \times \left(\frac{\vec{\nabla}s}{|\vec{\nabla}s|^2 + (s-m)^2} + \frac{\vec{\nabla}m}{|\vec{\nabla}m|^2 + (s-m)^2} \right). \tag{3}$$

In our implementation, equation (3) replaced the right side of equation (1) in calculating the demons force. The term 'passive' force was used to emphasize the contribution of the gradient information from the static (reference) image. Similarly, the term 'active' force in equation (2) was used to emphasize that the gradient information of the deforming (moving) image is used. The term 'active' is more appropriate because the equation is solved iteratively and the moving image is deformed (and varies) during this process. Because of this new demons force, the algorithm converges more quickly and requires fewer iterations.

2.4. Multiresolution approach

One of the assumptions made in deriving the force calculation in equation (1) was that the deformation should be reasonably small. This is not always the case in clinical situations. One way to minimize the effect of large deformations is to use a coarse-to-fine multiresolution approach (Kostelec *et al* 1998). This approach uses low-resolution images derived from the original image (usually a high-resolution volumetric CT image) to begin the iterative demons diffusion process. After the solution converges, the displacement field is passed to the next higher resolution as the starting solution. In this study, we usually started with a

transverse image size of resolution 256 × 256, and used a total of three scales, with the lowest resolution at 64 × 64. The number of scales used can be easily extended to 4–6 when a larger deformation is observed or a higher resolution is used in the original image. This pyramidal multiresolution approach not only reduced the need for small deformations between two images, but also improved convergence, thus significantly increasing the calculation speed. In addition, we also pre-processed our CT images and performed a rigid-body registration to make the alignment of the two images reasonably close. We used a simple thresholding technique to extract bony structures in the two images based on CT numbers and then used similarity measures (cross-correlation or mutual information) to find the best (first step) alignment.

Cachier *et al* (1999) proposed another normalization factor α that allows force strength to be adjusted adaptively in each iteration. We adopted a similar implementation in our algorithm in which equation (3) becomes the following:

$$\vec{u} = (m - s) \times \left(\frac{\vec{\nabla} s}{|\vec{\nabla} s|^2 + \alpha^2 (s - m)^2} + \frac{\vec{\nabla} m}{|\vec{\nabla} m|^2 + \alpha^2 (s - m)^2} \right). \tag{4}$$

From the relationship: $|\vec{\nabla} s|^2 + \alpha^2 (s - m)^2 \geqslant 2 \cdot |\vec{\nabla} s| \cdot \alpha \cdot |s - m|$, it can be shown that equation (4) is bounded by a step size of $\frac{1}{2\alpha}$ (Cachier *et al* 1999). A smaller α value can be initially used for relatively large deformations and the step size then reduced when the algorithm approaches convergence. This will further speed up convergence.

The effect and the impact of the σ^2 and α parameters were not investigated in this preliminary study. We have chosen $\sigma^2 = 1.0$ for the Gaussian filter and $\alpha = 0.4$ for the normalization factor based on our initial experience using many clinical CT images (abdominal, thoracic and head-and-neck treatment sites). We also fixed σ^2 and α when switching from one resolution level to the next.

We implemented our modified demons algorithm in C language using a personal computer with a 2.8 GHz Intel Xeon processor running Microsoft Windows. Patients' CT images were acquired through two institutional review board-approved protocols, in which each patient's anatomy was imaged by CT before radiation treatment while the patient was in the treatment position. One of the goals for these two studies was to quantify the anatomical changes during the course of radiation therapy using an in-room CT-on-Rails system (Court *et al* 2003, 2004, Barker *et al* 2004).

2.5. Validation studies

Quantitative validation of a deformable registration algorithm for medical images is very difficult because of the general lack of known solutions in clinical situations. In addition, deformable image registration is inherently degenerative since multiple solutions may exist for a given match of image intensity. The appearance of the image after deformable image registration can only serve as a qualitative preliminary assessment.

We evaluated the modified demons algorithm for deformable image registration in three ways: (1) by simulated deformation of patients' CT images, (2) by measurement in a deformable pelvis phantom and (3) by evaluation of algorithm-segmented anatomical structures in sequential CT images of the same patient. The first two methods were quantitative; the third method was qualitative (in this study). They are described in detail below.

2.5.1. Mathematically simulated deformation. Theoretically, an original CT image can be transformed so as to simulate a known deformation. However, arbitrarily introduced organ deformation may not represent clinical reality. Therefore, we chose to create a

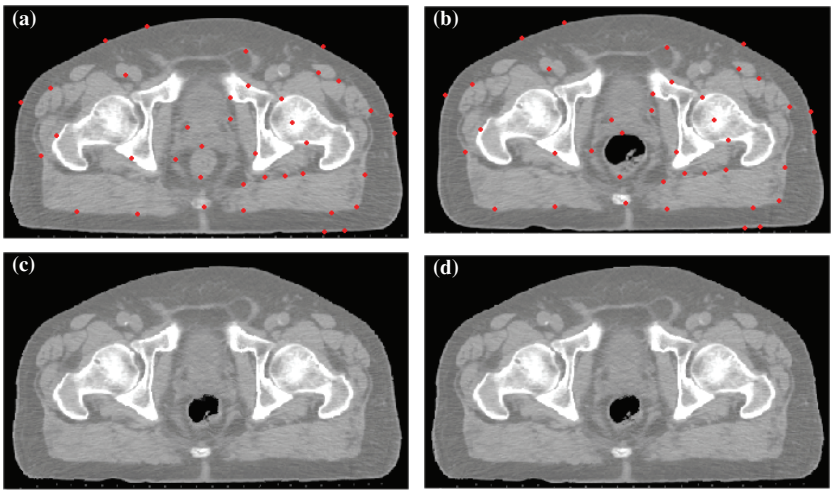

Figure 1. Mathematically deformed patient images. (a) Original reference image with control points shown for thin-plate spline (TPS) registration; (b) target image; (c) deformed image derived from (b) by TPS; (d) deformed image derived from (b) using the demons algorithm.

mathematical transformation in reference to sequential CT images of a patient during the course of radiation therapy. This allowed for quantitative validation of the deformable image registration algorithm in a clinical situation. Our approach was to use an alternative fiducial-based non-rigid transformation to register a pair of patient's CT images. The accuracy of this fiducial-based registration was not important for this study as long as the same deformation could be approximated in clinical situations. However, the resulting transformation itself was essential for introducing known deformations into the original image. Thereafter, the demons algorithm was used to deform the original image and match it with the mathematically transformed original image. This was a test of the ideal situation in which the greyscale intensity of an object in the CT images will not change over time even though the deformation may be significant.

We used a fiducial-based thin-plate spline (TPS) method (Bookstein 1989) to register a pair of sequential CT images of the same patient undergoing radiation therapy. This use of a real patient's CT images best represented the clinical situation in terms of daily patient anatomical variations, contrast, noise and artefacts in the CT images. It also allowed site-specific validations of the same technique at two different anatomical sites (i.e., the abdomen and head-and-neck regions).

The fiducial-based TPS method requires selection of homologous control points (fiducials) on the chosen patient CT image and the target CT image on the basis of anatomy. In our experience, a transformation based on well-defined homologous control points can produce a reasonably well-registered deformed image. Therefore, a combination of manual and automatic fiducial point selection was used.

Figure 1 illustrates mathematically transformed abdominal CT images. Two sets of CT images (figures 1(a) and (b)) from the same prostate cancer patient were acquired 7 days apart. Each of the images shown in figure 1 represents only one slice of a 3D CT data set. The homologous control points (red dots) were selected manually for the prostate and rectum and automatically for surrounding tissues and bony structures (Wang *et al* 2000). The image in figure 1(b) was deformed by the TPS method to match figure 1(a), thus producing

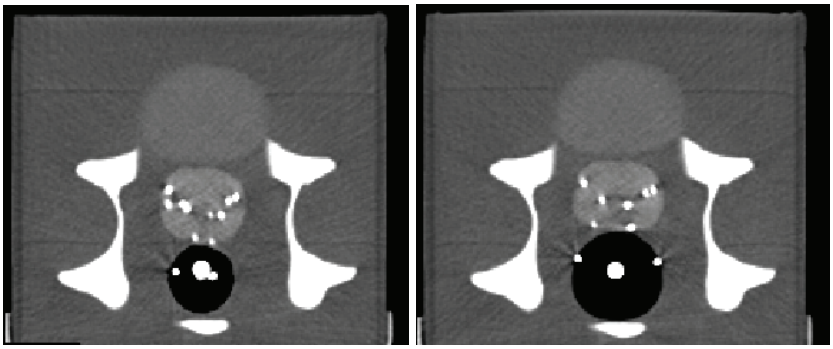

Figure 2. Deformable pelvis phantom containing simulated prostate, rectum, bladder, seminal vesicles and bony structures. (Left): Rectal balloon without inflation. (Right): Balloon inflated with 100 cc of air. Note displacement and deformation of the simulated prostate.

figure 1(c). With a known displacement field, figures 1(b) and (c) were used to validate the demons algorithm for deformable registration. The result of deformation by the demons algorithm is shown in figure 1(d). Although figure 1 shows only one slice of the 3D CT data set, all transformations in this research are three dimensional. Images were first cropped to a volume of interest (VOI) of 256 × 256 × 40 voxels in the transverse direction and the slice-thickness direction, respectively. For the prostate case, the voxel sizes were 0.94 mm × 0.94 mm × 3.0 mm; for the head-and-neck case, they were 0.68 mm × 0.68 mm × 3.0 mm.

2.5.2. Deformable pelvis phantom study. We designed a deformable pelvis phantom, which was then manufactured by CIRS, Inc. (Norfolk, VA). The phantom contained simulated prostate, bladder, seminal vesicles, rectum and bony structures with CT numbers matching our clinical CT images. The phantom was made of elastic materials by blending epoxy resins, urethanes, water-based polymers and other proprietary materials (CIRS, Inc., Norfolk, VA). Twenty-three plastic pellets from Beekley Corp (CT-SPOT^{TM}, Beekley Corp., Bristol, CT) were embedded in the prostate structure as markers for image registration. Each pellet had a diameter of 2.3 mm. These pellets served as markers to determine the deformation of the simulated prostate when an inflated rectal balloon was inserted into the phantom. We acquired a pair of phantom CT images before and after inflating the rectal balloon with 100 cc of air. The image pixel size was 0.94 mm, and the slice spacing was 3 mm. Figures 2(a) and (b) are the two images in the same CT slice. We used VariSeed^{TM} 7.1 software (Varian Medical Systems, Palo Alto, CA) to locate the seeds in both images. The correspondence of seeds in these two images was manually selected, and the displacement found by the software was used as the reference standard for validating the deformable registration algorithm.

2.5.3. Patient studies. To evaluate the demons algorithm in a situation as close as possible to the clinical situation, we performed deformable image registration for sequential CT images of the same patient. Because there were no known solutions in this situation, contoured anatomical structures in one of the early CT images were deformed and displayed on the later CT images using the same non-rigid transformation found by the demons algorithm. These deformed contours served to visually confirm the deformable transformation because the anatomical relationship of these segmented structures could be easily identified and compared with the same anatomy in the CT images.

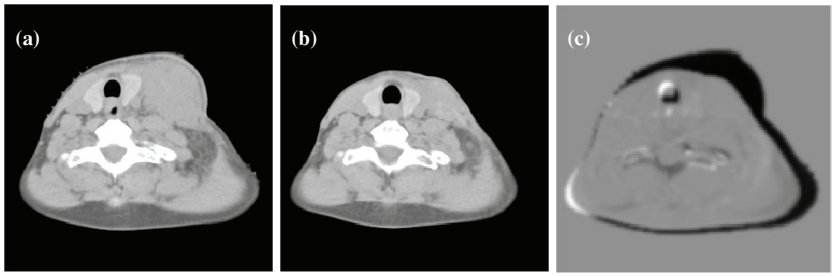

Figure 3. (a) One slice showing the original CT scan in a neck nodal region. (b) Same slice showing the second CT scan taken 37 days after the start of radiation treatment. Note clearly visible shrinkage of anatomy. (c) Difference image of (a) and (b).

Three cases were evaluated under these qualitative conditions by attending radiation oncologists. The first two cases consisted of sequential CT images of a prostate cancer patient and a head-and-neck cancer patient. The third case was a four-dimensional (4D) CT imaging study of a lung cancer patient that captured the tumour motion in ten breathing phases of approximately equal time interval. In this particular study, an attending radiation oncologist identified and contoured the tumour volume on only one phase (the end-of-expiration phase, being the most stable phase of all breathing cycles). This contoured structure was deformed to match the CT image obtained in the inspiration CT phase. The transformation matrix obtained from the deformable image registration by the demons algorithm was then used to transform the tumour contours from the end of expiration phase to the CT images from the inspiration phase. The contours were overlaid on the CT images from the inspiration phase to assess the accuracy of contour positions. We did not use the CT images obtained in any intermediate phases to register the deformable image; therefore, our studies constituted another test of organ deformation between two extreme breathing phases.

3. Results

3.1. Contribution of active force

We first tested the performance of the demons algorithm with the contribution of the active force on a pair of head-and-neck CT images. Figure 3 shows a pair of test images and their difference image. The first CT image (figure 3(a)) was acquired 10 days after the start of radiation treatment. The second CT image (figure 3(b)) was acquired on the last day of treatment (37 days after the first CT image). Figure 3(c) is the difference image between figures 3(a) and (b). A large anatomic change was apparent. These two CT scans were first aligned using rigid-body registration of bony structures (vertebral body). Figure 4 shows the incremental deformation at different iterations using the original demons algorithm (top row) and the modified demons algorithm (bottom row). In this case, the reference (static) image was the same as in figure 3(a), and the moving image was the same as in figure 3(b). It appears from the top row that voxels in regions of relatively larger distortion (external edge of the lymph node) were reluctant to move until the nearby field was built up from the edges. In contrast, the intensity flow was much faster along the high-gradient region (the edge of the body contour) than in the relatively uniform region near the centre of the field. This indicates that the original demons algorithm took an unnecessary path to achieve the final result. The bottom row of figure 4 shows selected intermediate steps from using the combined passive

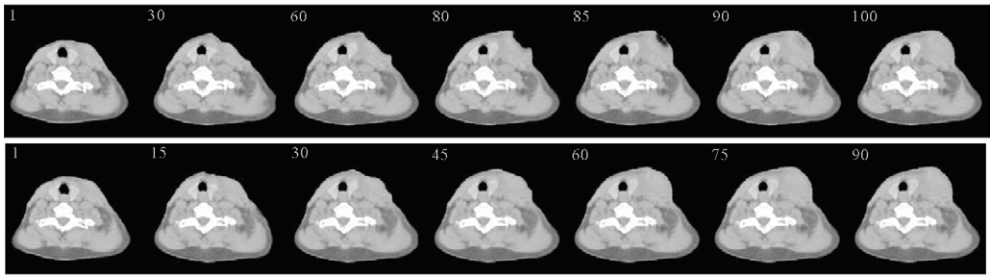

Figure 4. (Top row): Deformation of figure 3(b) to match figure 3(a) by means of the original demons algorithm. From left to right are the deformed images in iterations 1, 30, 60, 80, 85, 90 and 100. (Bottom row): Deformation of figure 3(b) to match figure 3(a) by means of an improved demons algorithm. From left to right are the deformed images in iterations 1, 15, 30, 45, 60, 75, 90.

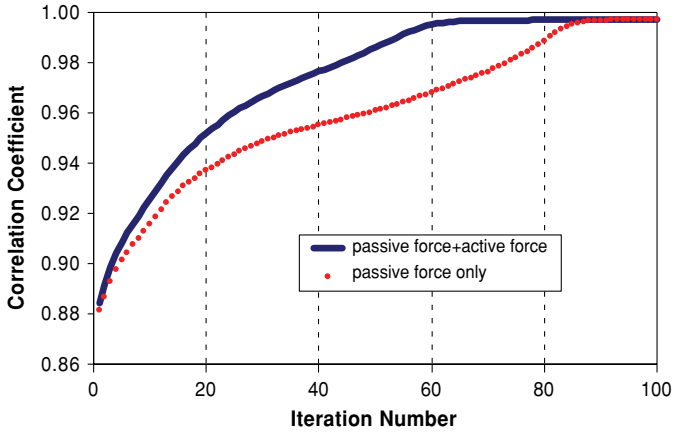

Figure 5. Correlation coefficient between reference image and deformed moving image as a function of iteration number for passive-force-only algorithm and the total-force algorithm.

and active forces to drive the deformation process. The lymph node appeared to 'grow' more realistically and correctly from the beginning because the active force on the skin line drove the deformation along the shortest distance in this region. As shown in figure 4, deformation in the demons algorithm converged at the 60th iteration (bottom row), compared with around the 100th iteration in the original algorithm (top row).

The efficiency of the active force implementation was also quantified with a similarity measurement. In figure 5, the correlation coefficient of the deformed image for each iteration is plotted. Assuming a correlation value of 0.995 (i.e., a good match between the deformed image and the original image), the passive force-based 'demons' algorithm converged around the 85th iteration, while the modified algorithm using both passive and active forces converged around the 60th iteration. Although the correlation coefficient had already reached 0.995 for the passive force-based algorithm at iteration 85, the deformation process appears incomplete until the 100th iteration (see top row of figure 4). In this test, we found that the computational cost of calculating active force was only 3% more; however, overall performance showed a 40% improvement when adding the active force.

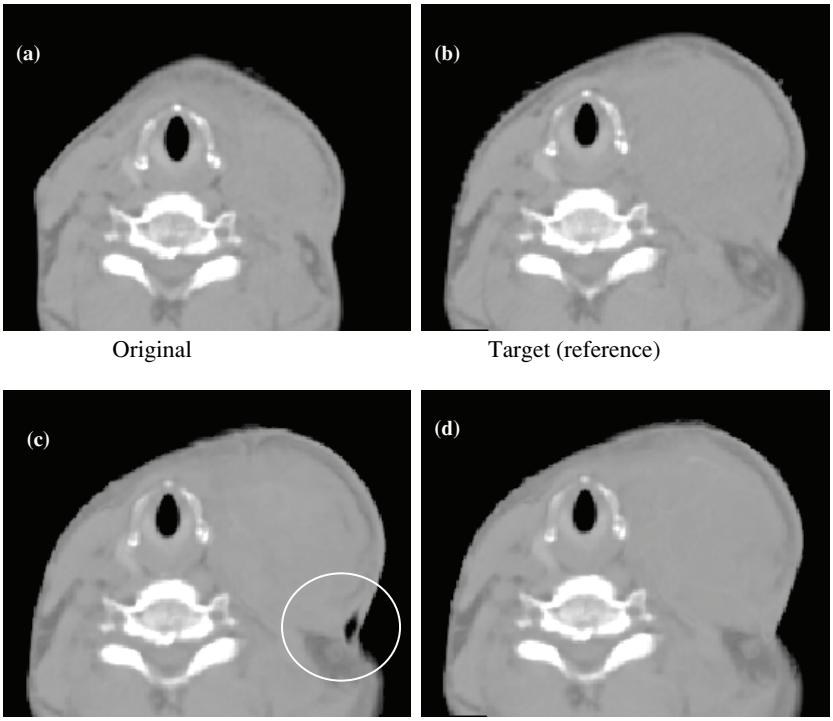

Figure 6. An example demonstrating that with the addition of 'active force' in the demons algorithm, better convergence can be achieved when relatively large deformations exist between a pair of images. (a) The original CT slice; (b) the target (reference) CT; (c) resultant CT image deformed from (a) to match with (b) using the passive-force only demons algorithm. Notice the circled area, in which the algorithm did not converge and left a hole in the area; (d) resultant CT image obtained by using both passive and active forces demons algorithm. The image in (d) matched well with the reference image in (b), demonstrating a superior performance by the implemented demons algorithm.

In addition to the speed improvement, we also found the implemented demons algorithm (with active force) performed better if all other conditions remained the same. Figure 6 shows the same head-and-neck example but at a different CT slice position. Both images (c) and (d) were deformed from the source image (a) to match with the target image (b). It can be seen that the deformed image (c) using the passive-force only demons algorithm still has a hole to fill in the circled area. Using our implemented demons algorithm with both active and passive forces, the deformed image (d) is much closer to the target image (b).

3.2. Simulated deformation of patient CT images

Figure 7(a) shows the distribution of the absolute error as a percentage of total points exceeding the error for the simulated prostate deformation using known non-rigid transformation. When we evaluated a subvolume (approximately 10 × 8 × 7 cm) around the prostate where the deformation occurred, we found that over 96% of the voxels were within 2 mm of the corresponding voxels in the destination image. The root-mean-square (rms) differences were

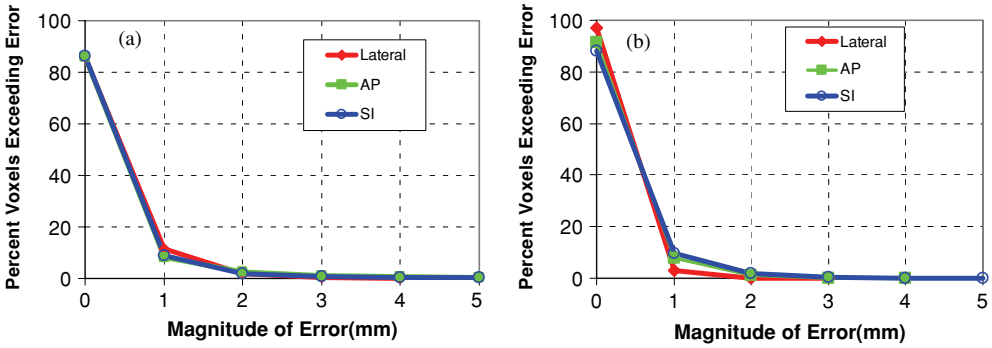

Figure 7. Summary of deformable registration errors in (a) mathematically deformed prostate patient CT images and (b) mathematically deformed head-and-neck patient CT images.

0.8 mm, 1.1 mm and 0.7 mm in the right–left (RL), anterior–posterior (AP) and superior–inferior (SI) directions, respectively. The mean and standard deviation for the magnitude of error were 0.5 mm $\pm$ 1.5 mm.

Similarly, for the head-and-neck case (which had a relatively large deformation), we evaluated a volume beneath the patient skin surface in the middle 30 CT slices. Since slices near the edge of the image data set in the superior–inferior direction provide insufficient information for registration, we excluded the first five slices and the last five slices in the analysis. Greater than 99% of the voxels were within 2 mm (figure 7(b)), with the largest errors occurring near the skin surface. The first row in figure 8 shows three slices of the head-and-neck CT image: one from the source CT image, one from the CT image deformed using the TPS technique, and one from the deformed image by the demons algorithm (The original CT images for the same case are shown in figure 3.). The middle row in figure 8 shows the introduced (known) displacements in the RL, AP and SI directions, overlaid on the demons algorithm-deformed image. The colours in three directions indicate that the lymph node expanded towards the patient's left, anterior and inferior sides. The maximum lateral shifts were 4.5 mm, 6.4 mm and 3.2 mm for voxels on the displayed image slice in the lateral, anterior and inferior directions. The third (bottom) row of figure 8 shows the residual shifts (errors) after deformable image registration using the demons algorithm. It can be seen that the displacement was considerably reduced, with most of residual errors occurring near the skin surface. The maximum error for this slice was 3.5 mm in the SI direction at a voxel near the skin surface. The spatial resolution of CT images in the SI direction (slice spacing) was 3 mm for this example.

The magnitude of displacement in the simulated deformed patient images, the demons algorithm-deformed images, and their errors are tabulated in table 1 for both the prostate and head-and-neck cases. Based on our experimental results on patient data, we used a Gaussian variance $\sigma^2 = 1.0$, i.e., fixed kernel size of $3 \times 3 \times 3$, and used fixed $\alpha = 0.4$ for both simulation cases.

3.3. Deformable pelvis phantom results

The displacement of implanted seeds detected by the deformable algorithm was compared with shifts detected by VariSeed software. After inflation of the rectal balloon, implanted seeds were shifted in three dimensions. Experiments showed that the demons algorithm can detect these three-dimensional shifts to within 0.8 ± 0.5mm. The maximum and minimum 3D shifts

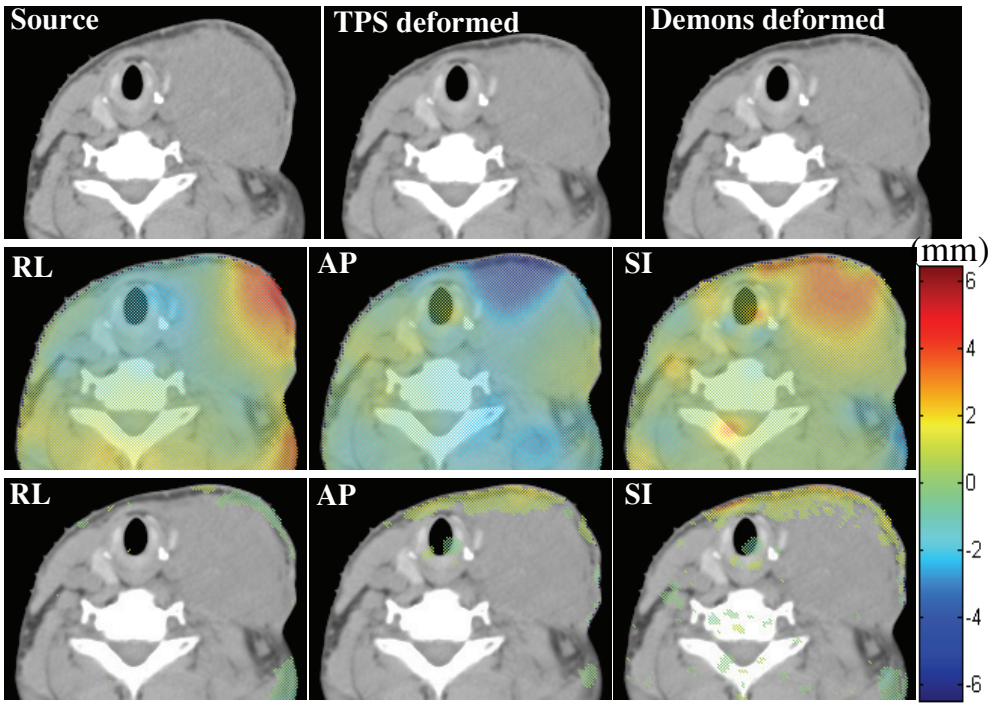

Figure 8. (Top row) (left): One slice of source image; (middle): corresponding slice of mathematically deformed image (used as a known solution); (right): same slice of demons-deformed image. (Middle row): Deformed image colourwashed with displacement. (Left): colourwashed with lateral displacement created by mathematical transformation; (middle): colourwashed with AP displacement; (right): colourwashed with SI displacement. (Bottom row): Deformed image colourwashed with residual errors of the deformable registration algorithm. (Left): colour overlaps with lateral error; (middle): colour overlaps with AP error; (right): colour-overlaps with SI error. All units are given in millimetres.

Table 1. Validation of deformable registration algorithm by comparing detected displacements with known displacements. The table shows the mean shift ±1 standard deviation.

	Known shifts	Demons-detected shifts	Mean residual error
Mathematically deformed prostate patient CT images[a]	3.5 ± 2.3 mm	3.2 ± 1.9 mm	0.5 ± 1.5 mm
Mathematically deformed head-and-neck patient CT images[b]	2.2 ± 1.2 mm	2.1 ± 1.2 mm	0.2 ± 0.6 mm
Deformable pelvis phantom[c]	6.5 ± 1.2 mm	5.9 ± 1.3 mm	0.8 ± 0.5 mm

[a] Evaluated on a 104 × 82 × 23 voxel region around the prostate target.
[b] Evaluated on a whole volume beneath the skin surface but excluding the most superior and inferior five CT slices.
[c] Evaluated on 23 seeds.

of these seeds were 9.0 mm and 4.5 mm. More details of using a deformable pelvis phantom to evaluate the deformable registration algorithm on prostate images were provided separately (Wang *et al* 2005). Detection errors and 3D shifts for the deformable pelvis phantom are also listed in table 1. Again, we used fixed Gaussian variance $\sigma^2 = 1.0$, and fixed $\alpha = 0.4$ for this case.

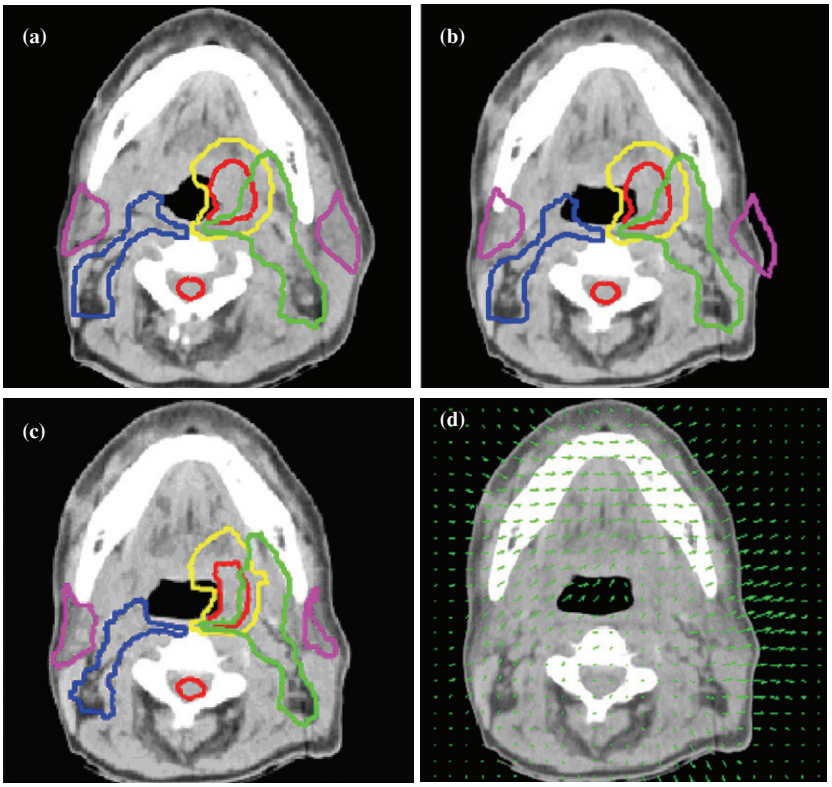

Figure 9. Autocontouring on head-and-neck images. (a) One slice of the planning CT with physician-drawn contour overlaid. (b) Corresponding slice on daily CT with planning contours directly overlaid. (c) Daily CT with deformed planning contours obtained by deformable registration algorithm. (d) Daily CT with displacement overlaid (scaled).

3.4. Patient studies

Figure 9 shows the validation of deformed contours for head-and-neck CT images. In this study, the same transformation generated by the demons algorithm was used to deform the original physician-drawn contours (figure 9(a)) to the new anatomy in later CT scans (figure 9(c)). The first CT scan was taken on January 15, 2003. A physician manually drew the contours for GTV (in red), left and right parotid gland (in magenta), primary CTV (in yellow), elective nodal CTV (in blue and green) and the spinal cord (in red). To illustrate the change in anatomy, we performed a rigid-body registration with bony structure alignment between the first CT scan and a later CT scan. The result is shown in figure 9(b). The original contours did not match up with the CT image of the patient's anatomy (mostly because of tissue shrinkage due to radiation treatment, but also in part because of a slight change in orientation of the mandible). When the deformable image registration algorithm was used to deform the original contours (figure 9(a)) to the new CT scan (figure 9(c)), the same contours matched much better. Radiation oncologists verified and confirmed the accuracy of these contours (in all CT slices). Figure 9(d) illustrates the displacement from figures 9(a)–(c) by showing the vector field that mapped the same volume element from the original CT image into the new position in the later CT.

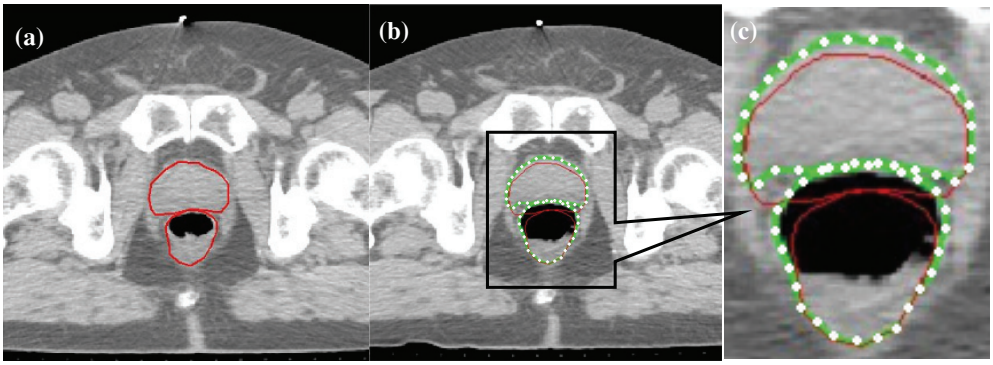

Figure 10. (Left): First daily CT with physician-drawn contours for prostate and rectum. (Middle): Second daily CT with first daily CT contours overlaid (red) and deformed contours by deformable registration (green with white dots). (Right): Centre part of middle image enlarged to show correction of deformed contours.

Similarly, figure 10 shows the validation of deformed contours for a pair of prostate CT images acquired 1 week apart. A radiation oncologist contoured the original CT scan in figure 10(a). Figure 10(b) shows two sets of contours, both derived from the original contours shown in figure 10(a): one from the rigid bony registration of the later CT with the original CT (shown in red), and the other from the contour deformation generated by the demons algorithm (shown in green with white dots to improve visualization). Again, the deformed contours matched much better with the image of the new anatomy. Figure 10(c) is an enlarged view of figure 10(b), showing that the deformed contour lines matched the enlarged rectum and the anteriorly displaced prostate much better than the rigid registration contours did.

Similarly, figure 11 shows one example of tracking the lung tumour motion in retrospectively reconstructed 4D CT images between two extreme breathing phases: the expiration phase (left column of figure 11) and the inspiration phase (middle and right column of figure 11). The three rows in figure 11 represent three different axial CT slice positions in each of the two breathing phases. The left column shows three slices of the end-expiration images and the physician-drawn contours of a tumour. The middle column shows the direct contour overlaid at the same slice position at the inspiration phase. It can be seen that the same contours drawn on the CT images from the expiration phase did not match up well with the tumour in the CT images from the inspiration phase. The images in the right column are the same CT images from the inspiration phase but overlaid with the deformed contours of the tumour from the expiration CT images. Although qualitative, the deformed contours in the right column of figure 11 agree with the CT images much better. The 3D nature of the objects involved and the deformation of lung tissues in different breathing phases made it almost impossible to pick the CT slice containing the same anatomy. Nevertheless, we demonstrated that deformable image registration could be used to track tumour and lung motion in 4D CT images.

3.5. Computational performance

In general, the computing time to perform a deformable image registration using our demons algorithm varies depending on the size of the CT images and the resemblance of the moving image relative to the original reference image (to a minor degree). For a typical $256 \times 256 \times 61$ CT data set, it usually takes 6 min to complete the registration on a single Pentium CPU running at 2.8 GHz.

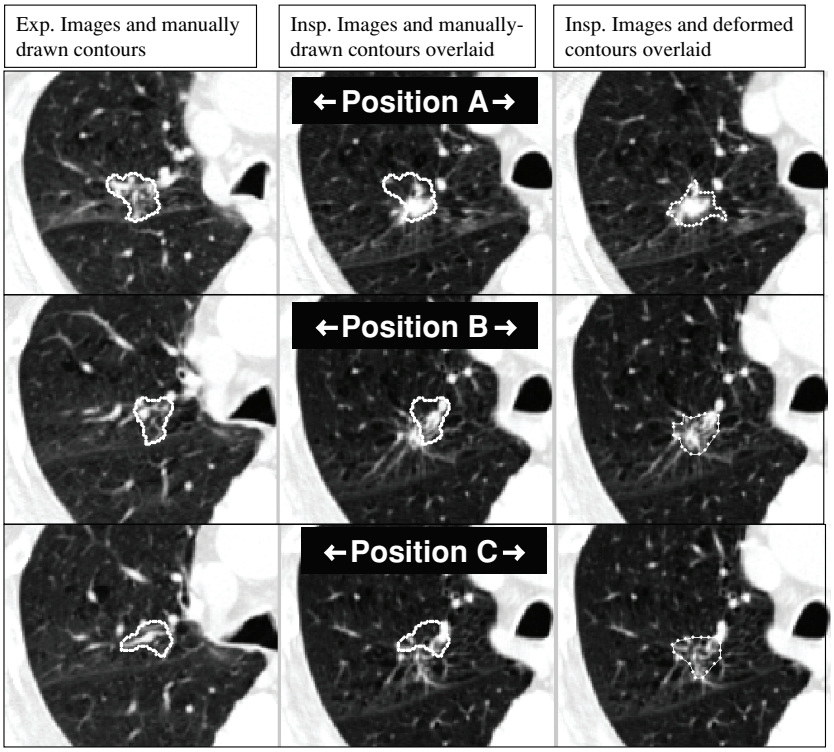

Figure 11. Tumour tracking in 4D CT images of thorax. Each row shows a different axial CT slice. (Left column): Three slices of CT images obtained in end-expiration phase with physician-drawn contours of the tumour. (Middle column): Same contours directly overlaid onto the inspiration CT images. (Right column): Same slices of inspiration CT images overlaid with deformed contours obtained by demons algorithm.

4. Discussion

In this study, we demonstrated that the demons algorithm (Thirion 1996, 1998) is an effective non-rigid registration technique for tracking anatomical variations within the same image modality. In its original implementation, the 'demons force' driving the image deformation was designed to occur only at voxels in the static reference image whose gradient was not zero. This was termed 'passive force' because the force was determined only by the greyscale image intensity of the reference image alone, without reference to the moving image (the destination image). Conversely, we demonstrated that an 'active' force derived from the intensity of the moving image could be used to effectively accelerate the algorithm. This 'active force' provided the added benefit of compensating for relatively large deformations between pairs of images. Although the multiresolution approach implemented in this study would have also provided the same benefit, the relative effects of the 'active force' and multi-resolution approaches were not studied.

Quantitative validation of a deformable image registration algorithm is difficult because of the general lack of known solutions in most situations. In this study, we designed three validation tests: the deformed patient images using alternative deformable registration methods, the use of fiducial markers in a deformable pelvis phantom and deformed contour studies. The first two tests are quantitative because known solutions are available. The third

test is qualitative since physicians were asked to confirm the delineated contours in the new anatomy. Although the test could have been made more quantitative if the physicians had been asked to draw these contours independently, it is also well known that there are intra- and inter-observer variations in manually delineated contours. Therefore, we did not perform such a comparison in this study, although we just started conducting an independent study of inter-observer variation in contouring head-and-neck anatomy that may define the accuracy requirement for a deformable image registration method.

It is also worth mentioning that we did not explicitly include topological information in our demons algorithm. Instead, Gaussian regularization was used to smooth the displacement fields, especially in featureless regions (with uniform image intensities). A Gaussian filter with larger variance was found to be effective in alleviating the effect of noise and preserving the topology of normal structures. However, higher variance slowed down the convergence of the algorithm. Bro-Nielsen and Gramkow (1996) have shown that Thirion's demons algorithm is similar to the viscous fluid-based algorithm except that the elastic filter is replaced by a Gaussian filter. We did not compare our model with other biomechanical models that directly simulate organ deformation by taking advantage of the physical properties of tissues (e.g., elasticity) (Liang and Yan 2003, Yan *et al* 1999, Lockman *et al* 2000, Yan and Lockman 2001, Brock *et al* 2002, 2003). For example, Yan *et al* (1999) used a finite element method and tissue elasticity to calculate the organ deformation based on a set of pre-determined common boundary points. Brook *et al* (2002) used a similar technique to study liver deformation and dose tracking. Public domain software available is also available for performing non-rigid registration, mainly for brain image mapping. For example, AIR programs (automated image registration, developed by Dr Roger P Woods, at University of California Los Angles (UCLA), http://bishopw.loni.ucla.edu/) can do homologous deformable registration using polynomial basis functions (Woods *et al* 1998a, 1998b). However, low order polynomials may not be able to adapt well local deformations and high order polynomials tend to introduce spatial distortions. Therefore, a small field-of-view is recommended. The biomedical imaging group at Laboratoire d'imagerie biomédicale (LIB) (http://bigwww.epfl.ch/) in Switzerland developed intra-modality registration algorithms using a region-of-interest approach. The local deformation model used a combination of translation, rotation and affine transformations (Thevenaz *et al* 1998). The functional imaging laboratory at University of London developed statistical parametric mapping (SPM) tools (http://www.fil.ion.ucl.ac.uk/spm/), which also included a deformable model using a discrete cosine basis set (Wright *et al* 1995, Ashburner and Friston 1999, 2000).

To quantify and track the time- and space-dependent variations in patient's anatomy, deformable image registration is necessary to map the position of each volume element on all CT images to a reference CT image. This reference image is preferably the planning CT image from which the original treatment plan was designed. This allows the actual dose distributions to be compared with the original planned distribution. Using a deformable image registration method, the dose to each voxel can be accumulated. In the present study, we focused on implementing our demons deformable registration algorithm. We tested the algorithm for a head-and-neck case (figure 9), a prostate case (figure 10) and a lung cancer case (figure 11). More cases have been done so far with similar results. We plan to conduct dose tracking studies in the near future.

A number of deformable image registration research studies related to radiotherapy applications have been reported in the literature. Using selected control points from physician-drawn contours on each CT image, Schaly *et al* (2004) mapped deformable daily anatomies back to the planning CT and used TPS-based transformations to track doses. However, the uncertainties of selecting fiducial points can introduce non-trivial misregistration (Liang and

Yan 2003). Other image-based algorithms are also proposed. Christensen *et al* (2000) utilized a 'fluid registration' technique, and others have used 'optical flow' methods (Barron *et al* 1992, Lai and Vemuri 1998, Vemuri *et al* 1998). Recently, Lu *et al* (2004) proposed a free-form deformable image registration algorithm that utilizes a calculus of variations. Their formulation of the final partial differential equation was similar to the demons implementation, but their force calculation was different from ours (equation (4)). Lu *et al* also compared their approach to a version of the demons algorithm using synthetically deformed prostate CT images, which may have no correlation to physical reality. Although they found that their method was superior to the demons algorithm at higher-order harmonics and at large distortions, it was not clear whether the parameters they used in the demons algorithm were optimal for their test cases. In addition, synthesized and severely deformed CT images may be extreme for testing these algorithms because they are not realistic in clinical situations.

Although qualitative, our validation of the demons algorithm by deforming the original contours to subsequent CT images of the same patient has important implications. Because the same displacement field found by the demons algorithm is used to transform these contours, our validation method should be useful for checking the accuracy of a deformable image registration algorithm *in vivo*. In addition, we also solved an important problem of delineating daily target volumes and critical normal organ structures for daily CT-guided adaptive radiotherapy. Computer-based auto-contouring of target volumes and critical structures would be greatly simplified if the previously drawn contours were available. This is usually the case in CT-guided radiation therapy, since it is necessary to draw contours on the planning CT images before designing the initial radiation treatment plan. By deforming the original contours, one can track the doses delivered daily to the same structures or modify the treatment plan to adapt to the new anatomical shapes. This would eliminate the unrealistic need for oncologists to contour treatment targets, critical structures, or both, daily. We plan to continue our research in this area and test more patient cases in the future.

5. Conclusion

We implemented an effective deformable image registration technique using the demons algorithm for CT-guided radiation therapy. The algorithm was quantitatively validated to within $\sim$1.5 pixels in simulated patient CT images and in a deformable pelvis phantom. Radiation oncologists who had outlined the original contours visually verified the deformed contours and found them to be acceptable. Thus, the implemented demons algorithm may be an effective tool in CT-guided adaptive radiotherapy.

Acknowledgments

The authors would like to thank Tinsu Pan, who supplied the 4D CT images used in this experiment. The research was partially supported by the University of Texas MD Anderson Cancer Center start-up funds (Drs Cheung and Dong) and a seed grant from the University of Texas Center for Biomedical Engineering (Dr Dong).

References

Ashburner J and Friston K J 1999 Nonlinear spatial normalization using basis functions *Hum Brain Mapp* **7** 254–66
Ashburner J and Friston K J 2000 Voxel-based morphometry— the methods *Neuroimage* **11** 805–21

Barker J L Jr 2004 Quantification of volumetric and geometric changes occurring during fractionated radiotherapy for head-and-neck cancer using an integrated CT/linear accelerator system *Int. J. Radiat. Oncol. Biol. Phys.* **59** 960–70

Barron J L, Fleet D J, Beauchemin S S and Burkitt T A 1992 Performance of optical flow techniques *Proc. CVPR '92, 1992 IEEE Computer Society Conf. on Computer Vision and Pattern Recognition* pp 236–42

Bookstein F L 1989 Principal warps: thin-plate splines and the decomposition of deformations *IEEE Trans. Pattern Anal. Mach. Intell.* **11** 567–85

Brock K K, Hollister S J, Dawson L A and Balter J M 2002 Technical note: creating a four-dimensional model of the liver using finite element analysis *Med. Phys.* **29** 1403–5

Brock K K, McShan D L, Ten Haken R K, Hollister S J, Dawson L A and Balter J M 2003 Inclusion of organ deformation in dose calculations *Med. Phys.* **30** 290–5

Bro-Nielsen M and Gramkow C 1996 Fast fluid registration of medical images *Visualization in Biomedical Computing (VBC'96) Springer Lecture Notes in Computer Science (Hamburg)* pp 267–76

Cachier P, Pennec X and Ayache N 1999 Fast non-rigid matching by gradient descent: study and improvement of the 'Demons' algorithm *Technical Report* INRIA, RR-3706

Christensen G E, Yin P, Vannier M W, Chao K S C, Dempsey J F and Williamson J F 2000 Large-deformation image registration using fluid landmarks *Proc. Fourth IEEE Southwest Symposium on Image Analysis and Interpretation* pp 269–73

Court L, Rosen I, Mohan R and Dong L 2003 Evaluation of mechanical precision and alignment uncertainties for an integrated CT/LINAC system *Med. Phys.* **30** 1198–210

Court L E and Dong L 2003 Automatic registration of the prostate for computed-tomography-guided radiotherapy *Med. Phys.* **30** 2750–7

Court L E, Dong L, Taylor N, Ballo M, Kitamura K, Lee A K, O'Daniel J, White R A, Cheung R and Kuban D 2004 Evaluation of a contour-alignment technique for CT-guided prostate radiotherapy: an intra- and interobserver study *Int. J. Radiat. Oncol. Biol. Phys.* **59** 412–8

Ezzell G A, Galvin J M, Low D, Palta J R, Rosen I, Sharpe M B, Xia P, Xiao Y, Xing L and Yu C X 2003 Guidance document on delivery, treatment planning, and clinical implementation of IMRT: Report of the IMRT subcommittee of the AAPM radiation therapy committee *Med. Phys.* **30** 2089–115

Ford E C, Chang J, Mueller K, Sidhu K, Todor D, Mageras G, Yorke E, Ling C C and Amols H 2002 Cone-beam CT with megavoltage beams and an amorphous silicon electronic portal imaging device: potential for verification of radiotherapy of lung cancer *Med. Phys.* **29** 2913–24

Fung A Y, Grimm S Y, Wong J R and Uematsu M 2003 Computed tomography localization of radiation treatment delivery versus conventional localization with bony landmarks *J. Appl. Clin. Med. Phys.* **4** 112–9

Guimond A, Roche A, Ayache N and Meunier J 2001 Three-dimensional multimodal brain warping using the demons algorithm and adaptive intensity corrections *IEEE Trans. Med. Imaging* **20** 58–69

Hector C L, Webb S and Evans P M 2000 The dosimetric consequences of inter-fractional patient movement on conventional and intensity-modulated breast radiotherapy treatments *Radiother. Oncol.* **54** 57–64

Jaffray D A and Siewerdsen J H 2000 Cone-beam computed tomography with a flat-panel imager: initial performance characterization *Med. Phys.* **27** 1311–23

Jaffray D A, Siewerdsen J H, Wong J W and Martinez A A 2002 Flat-panel cone-beam computed tomography for image-guided radiation therapy *Int. J. Radiat. Oncol. Biol. Phys.* **53** 1337–49

Joshi S, Pizer S, Fletcher P T, Yushkevich P, Thall A and Marron J S 2002 Multiscale deformable model segmentation and statistical shape analysis using medial descriptions *IEEE Trans. Med. Imaging* **21** 538–50

Joshi S C and Miller M I 2000 Landmark matching via large deformation diffeomorphisms *IEEE Trans. Image Process.* **9** 1357–70

Kostelec P J, Weaver J B and Healy D M 1998 Multiresolution elastic image registration *Med. Phys.* **25** 1593–604

Lai S-H and Vemuri B C 1998 Reliable and efficient computation of optical flow *Int. J. Comput. Vis.* **29** 87–105

Li J G and Xing L 2000 Inverse planning incorporating organ motion *Med. Phys.* **27** 1573–8

Liang J and Yan D 2003 Reducing uncertainties in volumetric image based deformable organ registration *Med. Phys.* **30** 2116–22

Lockman D M, Yan D and Wong J 2000 Estimating the dose variation in a volume of interest with explicit consideration of patient geometric variation *Med. Phys.* **27** 2100–8

Lu W, Chen M-L, Olivera G, Ruchala K and Mackie T R 2004 Fast free-form deformable registration via calculus of variations *Phys. Med. Biol.* **49** 3067–87

Mackie T R *et al* 2003 Image guidance for precise conformal radiotherapy *Int. J. Radiat. Oncol. Biol. Phys.* **56** 89–105

Metaxas D N and Kakadiaris I A 2002 Elastically adaptive deformable models *IEEE Trans. Pattern Anal. Mach. Intell.* **24** 1310–21

Meyer C R, Boes J L, Kim B, Bland P H, Zasadny K R, Kison P V, Koral K, Frey K A and Wahl R L 1997 Demonstration of accuracy and clinical versatility of mutual information for automatic multimodality image fusion using affine and thin-plate spline warped geometric deformations *Med. Image Anal.* **1** 195–206

Rogelj P and Lovacic S 2003 Symmetric image registration *SPIE-Medical Imaging 2003: Image Processing* vol 5032 ed J M F Milan Sonka (San Diego, CA) pp 334–43

Samuelsson A, Mercke C and Johansson K A 2003 Systematic set-up errors for IMRT in the head and neck region: effect on dose distribution *Radiother. Oncol.* **66** 303–11

Schaly B, Kempe J A, Bauman G S, Battista J J and Van Dyk J 2004 Tracking the dose distribution in radiation therapy by accounting for variable anatomy *Phys. Med. Biol.* **49** 791–805

Sidhu K *et al* 2003 Optimization of conformal thoracic radiotherapy using cone-beam CT imaging for treatment verification *Int. J. Radiat. Oncol. Biol. Phys.* **55** 757–67

Stroom J C and Heijmen B J 2002 Geometrical uncertainties, radiotherapy planning margins, and the ICRU-62 report *Radiother. Oncol.* **64** 75–83

Thevenaz P, Ruttimann U E and Unser M 1998 A pyramid approach to subpixel registration based on intensity *IEEE Trans. Image Process.* **7** 27–41

Thirion J P 1996 Non-rigid matching using demons *Proc. CVPR '96, 1996 IEEE Computer Society Conf. Computer Vision and Pattern Recognition* pp 245–51

Thirion J P 1998 Image matching as a diffusion process: an analogy with Maxwell's demons *Med. Image Anal.* **2** 243–60

Tichavsky P and Wong K T 2002 New fluid-mechanics-based statistical models of a nominally linear towed-array's shape deformation *2002 IEEE International Conf. on Acoustics, Speech, and Signal Processing* vol 3 pp 2841–4

Valverde F L, Guil N, Munoz J, Li Q, Aoyama M and Doi K 2001 A deformable model for image segmentation in noisy medical images VO—3 *Proc. 2001 Int. Conf. on Image Processing* vol 3 pp 82–85

Vemuri B C, Huang S, Sahni S, Leonard C M, Mohr C, Gilmore R and Fitzsimmons J 1998 An efficient motion estimator with application to medical image registration *Med. Image Anal.* **2** 79–98

Wang H, Dong L, Lii M F, Lee A, Crevoisier d R, Mohan R, Cox J D, Kuban D and Cheung R 2005 Implementation and validation of a 3-dimensional deformable registration algorithm for targeted prostate cancer radiotherapy *Int. J. Radiat. Oncol. Biol.* **61** 725–35

Wang H, Zheng B, Good W and Zhuang T 2000 Thin-plate spline based automatic alignment of dynamic MR breast images *Proc. 22nd Annual Int. Conf. of the IEEE* vol 4 *(Chicago)* pp 2850–3

Woods R P, Grafton S T, Holmes C J, Cherry S R and Mazziotta J C 1998a Automated image registration-I-general methods and intrasubject, intramodality validation *J. Comput. Assist. Tomogr.* **22** 139–52

Woods R P, Grafton S T, Watson J D G, Sicotte N L and Mazziotta J C 1998b Automated image registration-II-intersubject validation of linear and nonlinear models *J. Comput. Assist. Tomogr.* **22** 153–65

Wright I C, McGuire P K, Poline J B, Travere J M, Murray R M, Frith C D, Frackowiak R S J and Friston K J 1995 A voxel-based method for the statistical analysis of gray and white matter density applied to schizophrenia *Neuroimage* **2** 244–52

Xie Z, Ng L and Gee J 2003 Two algorithms for non-rigid image registration and their evaluation *SPIE-Medical Imaging: Image Processing* vol 5032 ed J M F Milan Sonka (San Diego, CA) pp 157–64

Yan D, Jaffray D A and Wong J W 1999 A model to accumulate fractionated dose in a deforming organ *Int. J. Radiat. Oncol. Biol. Phys.* **44** 665–75

Yan D and Lockman D 2001 Organ/patient geometric variation in external beam radiotherapy and its effects *Med. Phys.* **28** 593–602